Rapid Communications

Probing the Jacobi shape transition in hot and rotating ^{43}Sc

Debasish Mondal,[1,*] Deepak Pandit,[1,2] S. Mukhopadhyay,[1,2] Surajit Pal,[1] Pratap Roy,[1,2] Vitisha Suman,[3] Balaram Dey,[4] Srijit Bhattacharya,[5] A. De,[6] C. Bhattacharya,[1,2] and S. R. Banerjee[1]

[1]*Variable Energy Cyclotron Centre, 1/AF-Bidhannagar, Kolkata-700064, India*
[2]*Homi Bhabha National Institute, Training School Complex, Anushaktinagar, Mumbai 400094, India*
[3]*Health Physics Division, Bhabha Atomic Research Centre, Mumbai 400094, India*
[4]*Department of Physics, Bankura University, Bankura 722155, India*
[5]*Department of Physics, Barasat Government College, Barasat, N 24 Parganas, Kolkata 700124, India*
[6]*Department of Physics, Raniganj Girls' College, Raniganj 713358, India*

(Received 8 September 2020; accepted 28 October 2020; published 18 November 2020)

The evolution of the hot and rotating ^{43}Sc nucleus to a highly deformed shape has been studied by measuring the high-energy γ rays from the decay of the giant dipole resonance. The compound nucleus was populated at two initial excitation energies and average angular momenta of $\approx$26 and 31$\hbar$ by using ^{16}O beam of energies $E_{\rm lab}$ = 120 and 142 MeV, respectively. The evaporated neutron energy spectra have been measured for proper determination of nuclear level density. The angular momentum has been determined by measuring the low-energy γ-ray multiplicities. The high-energy γ-ray and neutron spectra were analyzed simultaneously. At $\langle J\rangle \approx 26\hbar$ a near-oblate shape is observed, whereas at $\langle J\rangle \approx 31\hbar$ a sharp peak is observed at $E_\gamma \approx 10$ MeV pointing towards the transition to the Jacobi shape with quadruple deformation parameter $\beta \approx 0.7$. The results have been corroborated by the theoretical calculations based on the rotating liquid drop model framework.

DOI: 10.1103/PhysRevC.102.051302

The atomic nucleus is a many-body quantum system governed by the strong interaction among the constituent nucleons. However, many properties of the nucleus can be described by a macroscopic-microscopic model where the nucleus is assumed to be a macroscopic charged liquid drop or a more sophisticated system with a microscopic shell effect [1–5]. Due to the shell effect, the nucleus mostly has a prolate shape in the ground state and at low excitations rotates collectively in which the axis of rotation remains perpendicular to the symmetry axis. The shell effect melts above a temperature (T) of $\approx$2.0 MeV and a rotating nucleus assumes a noncollective oblate shape where the rotation axis coincides with the axis of symmetry. With the increase in angular momentum (J), the nucleus becomes more oblate deformed, and above a critical angular momentum (J_c), the shape changes to a highly deformed ($\beta > 0.6$) triaxial or a nearly collective prolate shape called the Jacobi shape. This shape transition was first suggested by Beringer and Knox [6] based on the observation of gravitational rotating systems, which under the influence of high angular momentum, change their shape from the so-called Maclaurin spheroid to a Jacobi ellipsoid. Later, many authors have theoretically predicted the shape transition for rotating nuclei based on semiclassical models [7–10]. It is observed that for mass number $A \gtrsim 180$, the nucleus undergoes fission with $J < J_c$, the value of which depends on the nuclear mass and charge [8,9]. Therefore, one could only observe the Jacobi shape transition experimentally in light and medium mass nuclei where J_c is much smaller than the critical angular momentum for fission.

Experimentally, the high-energy γ-ray line shape originating from the decay of the giant dipole resonance (GDR) [11,12] serves as an excellent tool to probe the shape of the nucleus at high T and J. Macroscopically, the GDR is described as the out-of-phase oscillation of proton and neutron fluids keeping a dipole shape. The resonance energy is inversely related to the axis length along which the vibration occurs, resulting in the splitting of the γ-ray line shape depending on the overall shape of the nucleus. The lifetime of the GDR being very small, it can also probe the shape of the nucleus at high T and J. However, the presence of thermal fluctuation at high excitations vitiates the signature of any shape transition [13–15] and it is difficult to draw any inference from only the γ-ray line shape. But, it has been shown, within the framework of the adiabatic thermal shape fluctuation model (TSFM) calculations, that the averaged absorption cross section gives a clear signature of the transition from a noncollective oblate to a highly deformed Jacobi shape in light mass nuclei [16]. It is also interesting to note that for light nuclei the rotational frequency for a given angular momentum is large as compared to that of heavy nuclei. This results in Coriolis splitting of the γ-ray line shape [17] and the three-component Lorentzian line shape for a collectively rotating deformed nucleus further splits into a five-component Lorentzian. The peak arising due to the vibration along the largest axis splits into two components, and a sharp peak is observed around $E_\gamma \approx 10$ MeV which is the unambiguous signature of the transition from noncollective oblate to the Jacobi shape. Apart from this

*debasishm@vecc.gov.in

low-energy peak, another signature of the Jacobi shape transition is a shoulder-like structure at $E_\gamma \approx 25$ MeV which was observed in ^{45}Sc [18] and ^{46}Ti [19,20]. The low-energy peak around $E_\gamma \approx 10$ MeV was first observed in ^{46}Ti where the high angular momentum events were properly selected [21,22]. In recent years, the Jacobi shape transitions have been observed in ^{47}V [23], ^{46}Ti [24], ^{31}P [25] where the sharp low-energy peak was clearly visible. It was also observed that the GDR line shape is quite different for an α-cluster nucleus compared to that of a non-α-cluster nucleus [23,25,26]. In this context, it should be mentioned that large deformation has also been observed in light mass nuclei from the measurement of light charged particles (LCPs) [27–31]. It was observed that to explain the LCP spectra with the statistical model calculations the yrast line had to be moved significantly downward compared to that of a spherical rigid nucleus. In Ref. [31], both the LCP and high-energy γ-ray spectra were measured for ^{46}Ti. It was observed that large deformation was required to explain the LCP spectra. However, no sharp peak at $E_\gamma \approx 10$ MeV was observed in the high-energy γ-ray line shape owing to the lack of high angular momentum events.

In this Rapid Communication, we report the evolution of ^{43}Sc to a highly deformed Jacobi shape by measuring the high-energy γ rays from the decay of the GDR. The energy spectra of the evaporated neutrons were also measured. The angular momentum of the compound nucleus (CN) has been determined properly by measuring the low-energy γ-ray multiplicities. The high-energy γ ray and evaporated neutron spectra have been analyzed simultaneously for proper determination of the nuclear level density (NLD) and other statistical model parameters along with the GDR absorption cross sections. The TSFM calculations have been performed to compare with the extracted GDR cross sections.

^{43}Sc was populated at $\approx$89 and 103 MeV excitation energies by bombarding a self-supporting ^{27}Al target with ^{16}O beam of energies 120 and 142 MeV, respectively, from the K-130 cyclotron at the Variable Energy Cyclotron Centre, Kolkata, India. The high-energy γ rays were detected by using a part of the LAMBDA array [32] consisting of 49 large BaF_2 scintillators. They were arranged in a 7×7 matrix which was placed at a distance of 50 cm from the target position at an angle of 90° with respect to the beam direction. The low-energy γ-ray backgrounds were removed by using a 5 mm thick passive lead shield in front of the array. The low-energy multiplicity γ rays were measured by using a multiplicity filter consisting of 50 small BaF_2 scintillators [33]. The multiplicity filter was divided into two 5×5 arrays of 25 scintillators each and placed on the top and bottom of the scattering chamber at a distance of $\approx$5 cm from the target position in a staggered castle-type geometry. Apart from measuring the γ-ray multiplicities, the multiplicity filters were used to generate the start trigger for time-of-flight (TOF) measurements. An event was recorded in a VME-based data acquisition system when, at least, one detector in the LAMBDA array above a threshold of $\approx$4 MeV fired in coincidence with, at least, one detector in both the top and the bottom multiplicity filter arrays. This technique selects the higher angular momentum space where the CN is likely to undergo Jacobi shape transition. Moreover, it helps in removing the background events significantly. The cyclotron rf time spectrum was also recorded with respect to the multiplicity signal to minimize the random backgrounds. The high-energy γ-ray spectra were reconstructed by using the cluster summing technique [32] with proper time and pulse shape discrimination (PSD) gates in each detector of the LAMBDA array. The time gate removes the neutron events, whereas the PSD gate rejects the pile-up events. The array was surrounded by a 10 cm thick passive lead shield to block the cosmic γ backgrounds, whereas the cosmic muon backgrounds were rejected using the hit patterns in the LAMBDA array, which are quite different from the actual γ events. The beam dump was situated at a distance of $\approx$3 m from the target. It was properly shielded with paraffin and lead blocks to minimize the backgrounds.

The evaporated neutrons were detected using a liquid scintillator (BC501A)-based detector placed at a distance of 150 cm from the target position at an angle of 150° with respect to the beam direction. The kinetic energy of the neutrons was determined by the TOF technique where the start signal was taken from the multiplicity filters and the prompt γ-γ peak was taken as the time reference. In each event, pulse shape was measured in addition to TOF to remove the γ backgrounds from the neutrons. The scattered neutrons were rejected by using the shadow bar technique. The final neutron spectra were then converted from the laboratory frame to the center-of-mass frame and were divided by the detector efficiency which was determined by the Monte Carlo computer code NEFF [34]. The detector efficiency at low energies (1–10 MeV) was also measured experimentally by using a ^{252}Cf source and was found to be in good agreement with the NEFF calculations.

As mentioned earlier, owing to the data acquisition condition (top-bottom coincidence of the multiplicity filters), slightly higher angular momentum events are selected. It was, therefore, crucial to determine the angular momentum distribution of the CN required for finding the average angular momentum populated in the CN as well as for statistical model calculations. In each event, the number of multiplicity filter fired simultaneously (called fold) was recorded and the angular momentum distribution was simulated from the measured fold distribution by using GEANT3 simulations [35]. The detailed procedure is described elsewhere [33]. In Fig. 1, the measured and simulated fold distributions are shown along with simulated angular momentum space which has been compared with that obtained from the PACE4 code.

The high-energy γ-ray absorption cross sections were extracted from the measured γ-ray spectra by the statistical model calculations using the statistical model code CASCADE [36] which is modified to include the γ decay from the GDR. The simulated angular momentum distribution was incorporated in the code and neutron, proton, α, and γ decays were considered. As mentioned earlier, the γ-ray strength function splits into five components due to Coriolis effect caused by high rotational frequency in light mass nucleus. Therefore, the partial decay width for γ rays was calculated by using the principle of detailed balance assuming a five-component

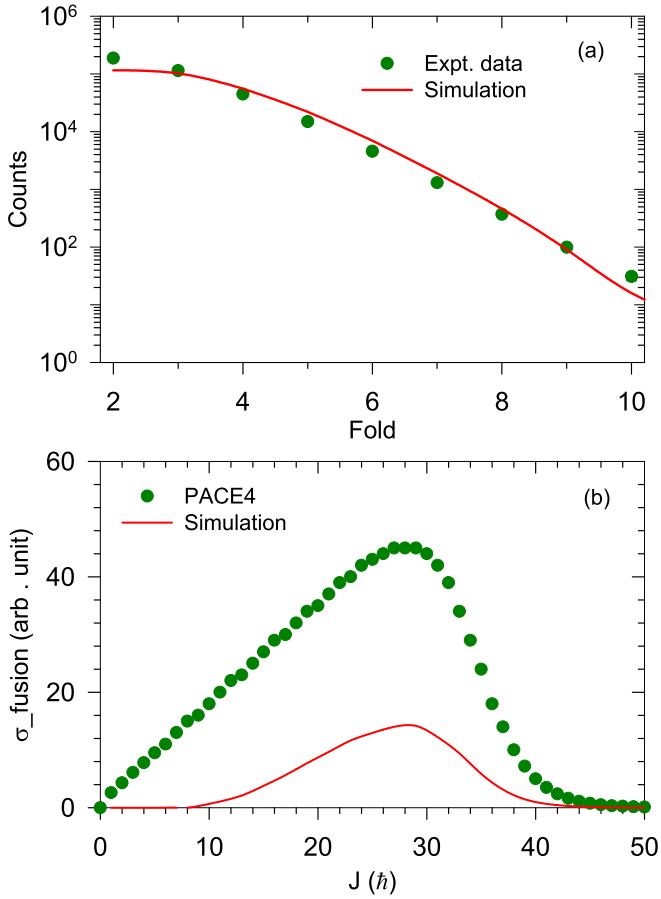

FIG. 1. (a) Measured (symbols) and simulated (line) fold distributions, (b) fusion cross sections obtained from the PACE4 code (symbols) and simulation (line) for $E_{\rm lab} = 120$ MeV and fold = 2.

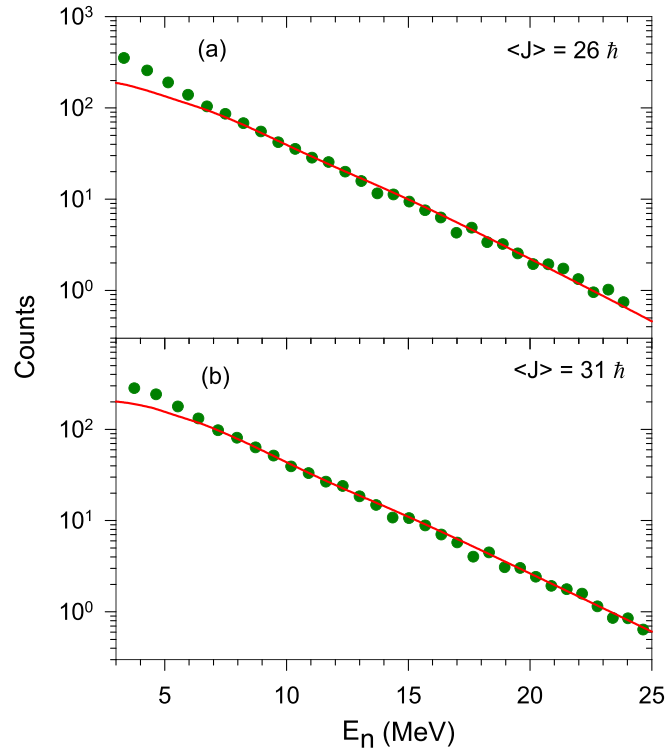

FIG. 2. Measured neutron energy spectra (symbols) along with the statistical model calculations (solid lines) for (a) $E_{\rm lab} = 120$ MeV and (b) $E_{\rm lab} = 142$ MeV. The error bars are within the symbols.

Lorentzian cross section given by

$$\sigma_{\rm abs}(E_\gamma) = \frac{4\pi e^2\hbar}{m_{\rm p}c}\frac{NZ}{A}\sum_{i=1}^{5}\frac{S_{\rm i}\Gamma_{\rm i}E_\gamma^2}{\left(E_\gamma^2 - E_{\rm i}^2\right)^2 + \Gamma_{\rm i}^2E_\gamma^2}, \quad (1)$$

where $E_{\rm i}$, $\Gamma_{\rm i}$, and $S_{\rm i}$ are the GDR energy, the width, and the GDR fraction of the total energy-weighted dipole sum rule, respectively, for individual components. $m_{\rm p}$ is the proton mass and N, Z, and A are neutron, proton, and mass numbers, respectively. One crucial component of the statistical model calculations is the NLD which has not been determined in earlier works. The level density is calculated by the Fermi gas model within which the NLD is governed by the level density parameter (LDP) (a). In the present calculations, the prescription for LDP put forward by Ignatyuk *et al.* [37] has been utilized. According to this prescription the LDP is given by $a = \tilde{a}(A)[1 + \frac{\Delta S}{U}\{1 - \exp(-\gamma' U)\}]$, where ΔS and γ' are the ground-state shell correction and shell damping factor, respectively. The asymptotic LDP is given by $\tilde{a}(A) = A/k$, k being the inverse level density parameter. As k depends on nuclear temperature and angular momentum [38,39], the high-energy γ-ray and the neutron spectra for a given excitation energy of the CN were analyzed simultaneously so that the GDR and the NLD parameters could be determined in a consistent way. It should be mentioned that a bremsstrahlung component, parametrized as $\sigma = \sigma_0 \exp(-E_\gamma/E_0)$, was added with the γ-ray spectra obtained from the CASCADE code to match with the experimental spectra. The parameters σ_0 and E_0 were determined by the visual inspection of the measured γ rays above $E_\gamma \approx 25$ MeV. We remark here that, in the earlier works [27–31], the nuclei were inferred to be highly deformed from the deformed yrast line required to fit the LCP spectra. The yrast line was parametrized by the effective moment of inertia (MI) $I_{\rm eff} = I_0(1 + \delta_1 J^2 + \delta_2 J^4)$, where I_0 is the spherical rigid body MI, δ_1 and δ_2 are the deformability coefficients. As the average angular momenta of the CN are $\gtrsim J_{\rm c} \approx 27\hbar$ [9], in the present Rapid Communication the statistical model calculations were performed using a deformed yrast line. It should be highlighted that unlike the LCPs, the slopes of evaporated neutron spectra are not much sensitive to the variation of the yrast line.

In Figs. 2 and 3 the experimental and the best-fit results of the statistical model calculations are shown for neutrons and high-energy γ rays, respectively. The linearized divided plots [Figs. 3(b) and 3(d)] are obtained by dividing both the experimental and the best-fit γ-ray spectra by a γ-ray spectrum calculated with a constant dipole strength of 0.2 W.u., where (W.u.) stands for the Weisskopf unit. We remark here that for $E_{\rm lab} = 120$ MeV, the high-energy γ-ray spectrum corresponding to the lowest available fold was selected. The average angular momentum in this case was $26\hbar$ which is just below the critical angular momentum $J_{\rm c}$. This spectrum could be fitted with a single-peak Lorentzian with an addi-

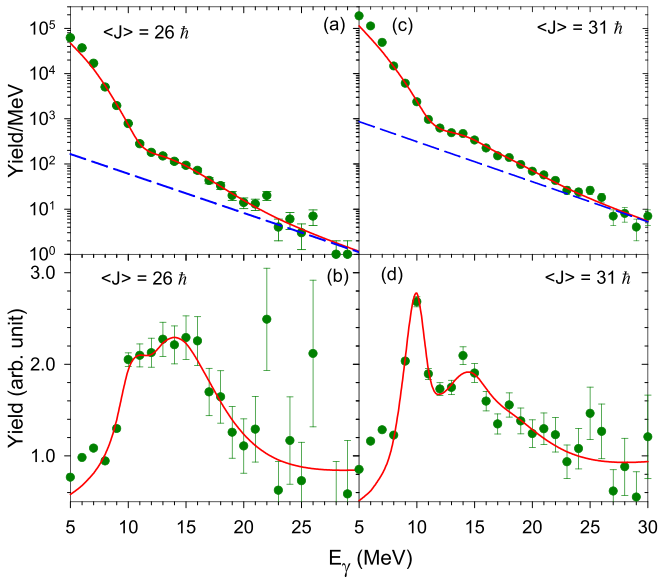

FIG. 3. Measured high-energy γ-ray spectra (symbols) along with the statistical model calculations (solid lines) for (a) $E_{\rm lab} =$ 120 MeV and (c) $E_{\rm lab} = 142$ MeV. The dashed lines are the bremsstrahlung components. (b) and (d) represent the corresponding linearized divided plots.

tional strength of $\approx$4% at $E_\gamma \approx 10$ MeV. However, a better fit was obtained by using an oblate-two-component Lorentzian with the previous mentioned strength at $E_\gamma \approx 10$ MeV. The low-energy strength at $E_\gamma \approx 10$ MeV appears due to a broad angular momentum distribution resulting in a fraction of CN states beyond J_c. On the other hand, a five-component Lorentzian with a strong peak at $E_\gamma \approx 10$ MeV was necessary to explain the high-energy spectrum at $\langle J\rangle = 31\hbar$. The best-fit parameters are shown in Table I. It is interesting to note that at both the cases the temperatures, i.e., the intrinsic excitations of the nucleus are the same.

The experimental observations are corroborated by the rotating liquid drop model calculations. As the shell effect vanishes at the temperature considered in this Rapid Communication, the free energy of a deformed rotating liquid drop is given by

$$F(T, J, \beta, \gamma, \Omega) = E_{\rm LDM}(\beta, \gamma) - TS(\beta, \gamma) + \frac{J(J+1)\hbar^2}{2(\hat{\omega}\cdot I\cdot\hat{\omega})}, \tag{2}$$

where $\hat{\omega}\cdot I\cdot\hat{\omega} = I_{\rm xx}\sin^2\theta\cos^2\phi + I_{\rm yy}\sin^2\theta\sin^2\phi + I_{\rm zz}\cos^2\theta$ is the MI about the rotation axis $\hat{\omega}$ and $\Omega = (\psi, \theta, \phi)$ are the Euler angles. The second term on the right-hand side of Eq. (2) does not vary much with deformation [16]. Therefore, for a nucleus rotating around the x axis,

$$F(J, \beta, \gamma) = E_{\rm LDM}(\beta, \gamma) + \frac{J(J+1)\hbar^2}{2I_{\rm xx}(\beta, \gamma)}, \tag{3}$$

The liquid drop energy ($E_{\rm LDM}$) has been calculated using the latest liquid drop model known as Lublin-Strasbourg drop model which properly takes care of the effect of the surface curvature [3]. The MI has been calculated using the relation $I_{\rm xx} = BI_{\rm sp}$, where $I_{\rm sp}$ is the MI of a spherical nucleus having the same volume as the deformed nucleus, $B = 0.5(a_y^2 + a_z^2)$, $a_x = \exp[\sqrt{(5/4\pi)}\beta\cos(\gamma + 2\pi/3)]$, $a_y = \exp[\sqrt{(5/4\pi)}\beta\cos(\gamma)]$, and $a_z = \exp[\sqrt{(5/4\pi)}\beta\cos(\gamma - 2\pi/3)]$. In this convention, $\gamma = 60^\circ$ and 0° represent the noncollective oblate and collective prolate shapes, respectively.

In Fig. 4, the free-energy surfaces are shown for different angular momenta. It is clearly observed, that with the increase in angular momentum, the minimum of the free-energy surface moves along the $\gamma = 60^\circ$ (y axis) and then proceeds towards $\gamma = 0^\circ$. This implies that ^{43}Sc has an oblate shape at low J; the deformation increases with the increase in J and then abruptly, it assumes a triaxial shape and move towards the collective prolate shape. The phenomenon can be easily understood from the polar plot on the β-γ plane (Fig. 5) where the minimum of the free-energy surface is plotted for different J values. It is observed that the noncollective oblate to triaxial shape change sets in at $J = 26\hbar$, which is quite similar to that obtained from the prescription of Ref. [9]. Moreover, the equilibrium deformation of ^{43}Sc at $J = 31\hbar$ is predicted to be $\beta \approx 0.7$.

In Fig. 6, the γ-ray absorption cross sections required to fit the high-energy γ-ray spectra have been shown along with the results of adiabatic TSFM calculations. Within this model the cross section at a given T and J is calculated as the weighted average of different cross sections corresponding to various deformations. The weight is given by $\exp(-F/T)$. The peak energies and widths of the GDR for a given deformation have been calculated by using the formalism of Junghans *et al.* [40], and the Coriolis splitting has been taken into account with the strength distributions as specified in Ref. [17]. As the absolute value of the absorption cross section has not been considered, the experimentally determined and theoretically calculated cross sections has been normalized by taking the area under the curves in the region $E_\gamma \approx$ 5–32 MeV. As could be seen from Fig. 6, the TSFM calculations qualitatively reproduce the γ-ray cross section determined from the statistical model calculations and its evolution with angular momentum. It is

TABLE I. The GDR and inverse level-density parameters at the specified temperatures and angular momenta.

$E_{\rm lab}$ (MeV)	$\langle J\rangle$ ($\hbar$)	T (MeV)	k (MeV)	E (MeV)	Γ (MeV)	S
120	26(6)	2.6(6)	7.8(3)	9.7(1)	2.0(1)	0.04(1)
				15.1(1)	8.6(2)	0.69(2)
				19.0(2)	11.0(4)	0.30(3)
142	31(6)	2.6(6)	8.0(2)	9.5(1)	2.0(1)	0.16(1)
				14.6(1)	4.6(2)	0.29(2)
				18.5(2)	6.5(4)	0.22(2)
				21.0(4)	8.3(5)	0.20(2)
				23.1(7)	11.0(9)	0.10(3)

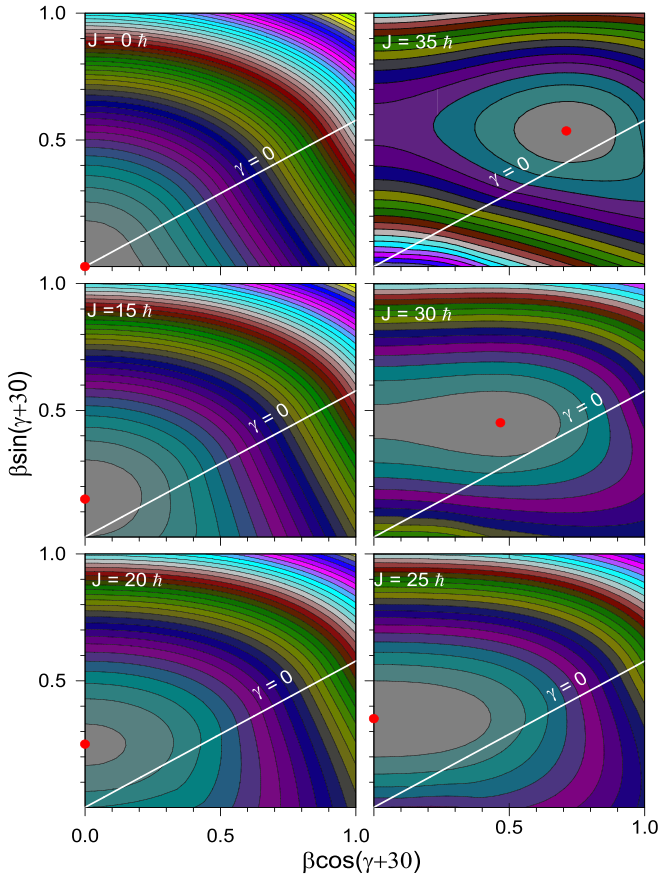

FIG. 4. Contour plots of the free-energy surfaces at the specified angular momenta. The symbols represent the minima of the free-energy surfaces.

evident that at $\langle J \rangle = 26\hbar$, ^{43}Sc nucleus roughly has an oblate shape. With the increase in angular momentum, the triaxiality increases resulting in a highly deformed Jacobi shape characterized by a strong peak at $E_\gamma \approx 10$ MeV at $\langle J \rangle = 31\hbar$. It is also evident that this shape transition is rather sharp which is corroborated by the rotating liquid drop model calculations (Fig. 5).

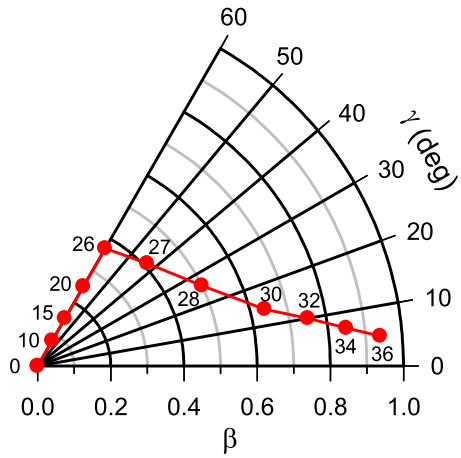

FIG. 5. Position of the free-energy minimum (filled circles) as a function of β and γ at different angular momenta mentioned.

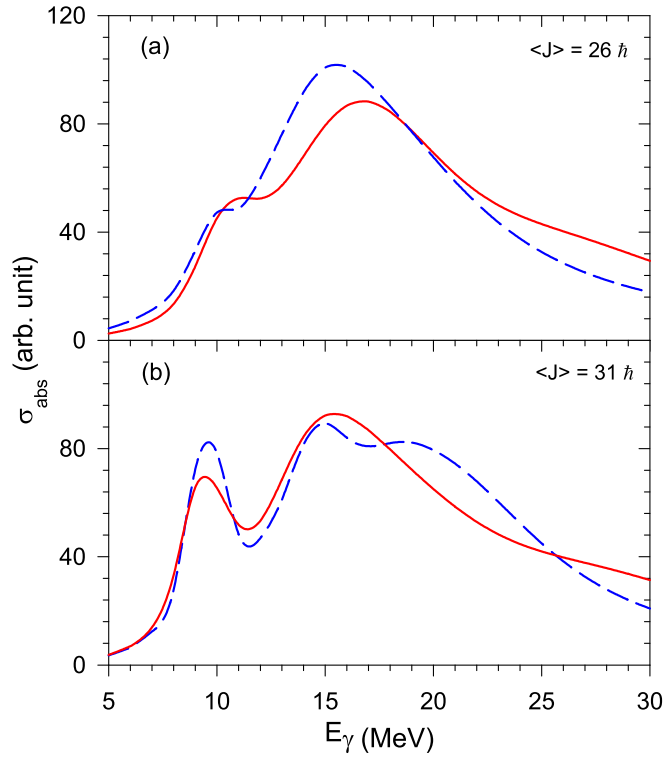

FIG. 6. The γ-ray absorption cross section incorporated in the CASCADE code (long-dashed lines) along with the TSFM calculations (solid lines) for (a) $E_{\rm lab} = 120$ MeV and (b) $E_{\rm lab} = 142$ MeV.

To summarize, the high-energy γ rays and evaporated neutrons have been measured from the decay of the ^{43}Sc nucleus populated at two different excitation energies. The angular momentum of the CN has been determined by measuring the low-energy γ-ray multiplicities. The high-energy γ-ray and evaporated neutron spectra were analyzed simultaneously to have a better control over the statistical model parameters. Near the critical angular momentum for the Jacobi shape transition, the nucleus roughly has an oblate shape, which evolves to a highly deformed Jacobi shape with quadruple deformation parameter $\beta \approx 0.7$ at $J \approx 31\hbar$. It is observed that the shape transition is rather sharp and the results are in good agreement with the theoretical calculations performed under the frameworks of the rotating liquid drop model and the adiabatic thermal shape fluctuation model. In the future, it will be interesting to probe the exotic shape transition by simultaneously measuring the high-energy γ rays, neutrons, and LCPs.

The authors are thankful to the VECC cyclotron staff for smooth running of the accelerator during the experiment. One of the authors (S.R.B.) acknowledges the financial assistance from the Science and Engineering Research Board, Government of India, Grant No. CRG-2018-000336.

[1] P. Möller *et al.*, At. Data Nucl. Data Tables **59**, 185 (1995).
[2] W. D. Myers and W. J. Swiatecki, Nucl. Phys. A **601**, 141 (1996).
[3] K. Pomorski and J. Dudek, Phys. Rev. C **67**, 044316 (2003).
[4] V. M. Strutinsky, Nucl. Phys. A **95**, 420 (1967).
[5] K. Pomorski, Phys. Rev. C **70**, 044306 (2004).
[6] R. Beringer and W. J. Knox, Phys. Rev. **121**, 1195 (1961).
[7] S. Cohen, F. Plasil, and W. J. Swiatecki, Ann. Phys. (NY) **82**, 557 (1974).
[8] A. J. Sierk, Phys. Rev. C **33**, 2039 (1986).
[9] W. D. Myers and W. J. Swiatecki, Acta. Phys. Pol., B **32**, 1033 (2001).
[10] K. Mazurek, J. Dudek, A. Maj, and D. Rouvel, Phys. Rev. C **91**, 034301 (2015).
[11] J. J. Gaardhøje, Annu. Rev. Nucl. Part. Sci. **42**, 483 (1992).
[12] M. N. Harakeh, A. van der Woude, *Giant Resonances: Fundamental High-Frequency Modes of Nuclear Excitiaion* (Clarendon Press, Oxford, 2001).
[13] D. R. Chakrabarty, M. Thoennessen, S. Sen, P. Paul, R. Butsch, and M. G. Herman, Phys. Rev. C **37**, 1437 (1988).
[14] Y. Alhassid, B. Bush, and S. Levit, Phys. Rev. Lett. **61**, 1926 (1988).
[15] D. Pandit, S. Bhattacharya, D. Mondal, B. Dey, S. Mukhopadhyay, S. Pal, A. De, and S. R. Banerjee, Phys. Rev. C **99**, 024315 (2019).
[16] Y. Alhassid and N. Whelan, Nucl. Phys. A **565**, 427 (1993).
[17] K. NeerGård, Phys. Lett. B **110**, 7 (1982).
[18] M. Kicińska-Habior *et al.*, Phys. Lett. B **308**, 225 (1993).
[19] A. Maj *et al.*, Nucl. Phys. A **687**, 192c (2001).
[20] A. Maj *et al.*, Acta. Phys. Pol., B **32**, 2433 (2001).
[21] A. Maj *et al.*, Nucl. Phys. A **731**, 319 (2004).
[22] M. Kmiecik *et al.*, Acta Phys. Pol., B **36**, 1169 (2005).
[23] D. Pandit *et al.*, Phys. Rev. C **81**, 061302(R) (2010).
[24] D. R. Chakrabarty *et al.*, Phys. Rev. C **85**, 044619 (2012).
[25] B. Dey *et al.*, Phys. Rev. C **97**, 014317 (2018).
[26] D. Pandit, D. Mondal, B. Dey, S. Bhattacharya, S. Mukhopadhyay, S. Pal, A. De, and S. R. Banerjee, Phys. Rev. C **95**, 034301 (2017).
[27] C. Bhattacharya *et al.*, Phys. Rev. C **65**, 014611 (2001).
[28] P. Papka *et al.*, Acta. Phys. Pol., B **34**, 2343 (2003).
[29] A. Dey, S. Bhattacharya, C. Bhattacharya, K. Banerjee, T. K. Rana, S. Kundu, S. Mukhopadhyay, D. Gupta, and R. Saha, Phys. Rev. C **74**, 044605 (2006).
[30] M. Kmiecik *et al.*, Acta Phys. Pol., B **38**, 1437 (2007).
[31] M. Brekiesz *et al.*, Nucl. Phys. A **788**, 224c (2007).
[32] S. Mukhopadhyay *et al.*, Nucl. Instrum. Methods Phys. Res., Sect. A **582**, 603 (2007).
[33] D. Pandit *et al.*, Nucl. Instrum. Methods Phys. Res., Sect. A **624**, 148 (2010).
[34] G. Dietze and H. Klein, Report No. PTB-ND-22, 1982 (unpublished).
[35] R. Brun *et al.*, GEANT3, CERN-DD/EE/84-1, 1986.
[36] F. Pühlhofer, Nucl. Phys. **280**, 267 (1977).
[37] A. V. Ignatyuk *et al.*, Yad. Fiz. **21**, 485 (1975) [Sov. J. Nucl. Phys. **21**, 255 (1975)].
[38] P. Roy *et al.*, Phys. Rev. C **94**, 064607 (2016).
[39] P. Roy *et al.*, Phys. Rev. C **86**, 044622 (2012).
[40] A. R. Junghans *et al.*, Phys. Lett. B **670**, 200 (2008).